Chemical Physics Letters 492 (2010) 44–48

Contents lists available at ScienceDirect

Chemical Physics Letters

journal homepage: www.elsevier.com/locate/cplett

Oxygen interstitial structures in close-packed metal oxides

Alexey A. Sokol, Aron Walsh *, C. Richard A. Catlow

University College London, Department of Chemistry, Materials Chemistry, Third Floor, Kathleen Lonsdale Building, Gower Street, London WC1E 6BT, United Kingdom

ARTICLE INFO

Article history:
Received 22 February 2010
In final form 14 April 2010
Available online 24 April 2010

ABSTRACT

We examine oxygen incorporation in alpha-Al_2O_3 using electronic structure techniques. We demonstrate that the ground-state configuration is a peroxide split interstitial, which is more than 2 eV *lower* in energy than the oxide closed-shell interstitial species in alumina, which proves to be only a transition state. Our results have general implications for the nature of oxygen interstitials in close-packed oxides.

1. Introduction

Metal oxides exhibit a diverse set of physicochemical properties. Virtually all applications are dependent on the underlying defect chemistry of the material, e.g. oxygen diffusion in solid-state electrolytes used in fuel cells and defects as active sites in heterogeneous catalysis, electronic, optical and electrical devices. Incorporation or loss of oxygen with its environment is one of the most fundamental defect processes that occurs in metal oxide systems [1]. The nature of the species found is, however, complex owing to the competing modes of incorporation of interstitial oxygen and the strong dependence on the oxygen oxidation state and spin.

Most common oxide structures are derived from a close-packed oxygen sublattice due to the comparatively large radius of the oxygen anion relative to metal cations from the upper part of the Periodic Table, e.g. rock-salt (MgO); fluorite (CeO_2); rutile (TiO_2); corundum (Al_2O_3); spinel ($MgAl_2O_4$) and perovskite ($SrTiO_3$). Interstitial oxygen species may form due to interaction with an oxygen rich environment, anion Frenkel pair formation, or through radiation damage.

Here we focus on α-alumina, an important dielectric material that is used in a variety of technological and catalytic applications and has been the focus of considerable experimental investigation, with particular emphasis on its mechanical and atomic transport properties [2–5]. Furthermore, many theoretical studies of defects in Al_2O_3 have been reported based on classical interatomic potential [6–10], semi-empirical [11–13], Hartree–Fock [14], density functional [15,16], and most recently hybrid density functional methods [17,18]. Many of these studies have focused on the F-centre associated with oxygen vacancy formation, while the nature of oxygen interstitial structure and spin configuration has received much less attention.

In this Letter, we demonstrate that alternate configurations for the neutral oxygen interstitial in the corundum lattice can change the defect formation energy by more than 2 eV. Furthermore, the energy hypersurface is highly sensitive to both the formal oxidation state and spin of the interstitial species. These results highlight the careful consideration that must be given to the treatments of defects in close-packed oxide systems; an accurate description of the equilibrium point defect properties is essential before ion transport or more complex defect reaction mechanisms can be investigated.

2. Methodology

Atomic and electronic structure of the defect states of interest have been modelled within a supercell approach (periodic boundary conditions) using a Density Functional Generalised Gradient Approximation level of theory (DFT-GGA). In this approach a single point defect, embedded in the ideal crystalline material, is placed in a large simulation cell that is periodically repeated on a three-dimensional lattice, which allows one to exploit standard periodic DFT codes. Thus, unfortunately, an artificial interaction of the defect with its periodic 'images' is introduced. Account and exclusion of such interactions from the calculated defect properties is extensively discussed in the current literature, particularly for charged defects that experience strong long-range effects and require large simulation cells [19]. An alternative approach would be to consider the point defects in the dilute limit as an embedded cluster, e.g. as implemented in the QM/MM Chemshell package [20,21]. Since we are concerned here only with well-localised charge neutral defects, the supercell needs not be excessively large. Nevertheless, the effect of defect–defect interactions can also be reduced by a judicious choice of the supercell shape, the cuboid being optimum, as it dampens slower decaying contributions to the energy and forces. We have constructed a cuboid cell, of 8.33 × 9.61 × 13.14 Å dimensions, that contains 120 atoms and is a fourfold anisotropic extension,

$$\begin{pmatrix} 2 & 0 & 0 \\ 1 & 2 & 0 \\ 0 & 0 & 1 \end{pmatrix},$$

* Corresponding author.
E-mail addresses: a.sokol@ucl.ac.uk (A.A. Sokol), a.walsh@ucl.ac.uk (A. Walsh), c.r.a.catlow@ucl.ac.uk (C.R.A. Catlow).

0009-2614/$ - see front matter © 2010 Elsevier B.V. All rights reserved.
doi:10.1016/j.cplett.2010.04.029

of the hexagonal unit cell of the corundum structure. We note that the crystallographic unit cell of corundum is rhombohedral, which is still three times smaller than the hexagonal setting.

In this study, we have employed the VASP code [22,23] with the PBE exchange and correlation functional [24], a PAW approximation used to describe core electrons [25], a 500 eV energy cut-off for the plane-wave expansion of the valence and conduction states, and the first Brillouin zone sampling using a $2 \times 2 \times 2$ k-point mesh. With the unit cell size used, the latter approximation provides reasonably converged densities for the wide-gap dielectrics, including α-alumina (E_g = 9.25 eV). The energy minima and the minimum-energy paths (obtained using the Nudged Elastic Band, NEB, method [26]) reported have been converged to 5 meV/Å for atomic forces.

In our defect calculations, we have relaxed only internal coordinates while keeping the supercell parameters fixed at the values optimised for the perfect structure of α-alumina as summarised in Table 1.

The calculated structural parameters are in good agreement with experiment, overestimated by less than 1.5 %, typical of the GGA. The optical band gap, in common with standard GGA calculations on oxide insulators, is underestimated by ca. 37%. Our investigation, however, focuses on the neutral oxygen interstitial, which is a strong electron acceptor characterised by defect levels in the lower part of the band gap of α-alumina, as discussed below. As the defect processes of interest prove to be much lower in energy than the calculated band gap value, we do not expect it to have a significant effect on our results.

3. Results and discussion

We consider the defect reaction involving the incorporation of a neutral oxygen atom from gaseous oxygen into the Al_2O_3 lattice (using the standard notation of Kröger and Vink):

$$V_i + \frac{1}{2}O_2(g) \rightleftharpoons O_i. \quad (1)$$

Thus, calculations of the defect formation energies do not need to include an oxygen atom in vacuum, which is not accurately described by the contemporary density functional theory.

The crystal structure of α-alumina can be represented as a stack of close-packed oxygen layers with octahedrally coordinated Al ions (shown in Fig. 1) in the ⟨0 0 1⟩ direction. In each layer, edge-sharing Al octahedra are arranged on a hexagonal lattice with one third of the lattice sites remaining vacant. These sites are designated as octahedral interstitials. In a different view, along the ⟨1 1 0⟩ direction, a closely-packed stack of face-sharing octahedral layers can be identified, in which octahedra occupy a rectangular lattice, again with every third site missing in rows running in the ⟨0 0 1⟩ direction. All Al sites in the corundum structure are symmetry equivalent and so are the O and octahedral vacant sites.

Our calculations initially placed an oxygen atom at the octahedral interstitial site, characterised by six O_i–O^{2-} distances of 2.00 Å and two O_i–Al distances of 1.94 Å, i.e. the octahedral site lies at the midpoint of a 'vertical' (c axis) vector connecting two symmetry equivalent Al sites situated in the adjacent (0 0 0 1) planes. The face-sharing pattern, in which the interstitial and two Al octahedra are related, results in the close proximity of these sites. As the neutral oxygen atom has a relatively small size (with a covalent radius of 0.68 Å), its electronic structure can be expected to retain essential features from the gas phase. Indeed, the valence shell of a neutral oxygen atom consists of one doubly and two singly occupied degenerate outer p-orbitals, which combine to give rise to a triplet ground-state in agreement with Hund's rules ([↑↓][↑][↑]). Flipping of spin on one of the singly occupied orbitals yields an excited open-shell (spin unrestricted) singlet state ([↑↓][↑][↓]), and a subsequent transfer of an electron from one singly occupied orbital to another results in a still higher-energy closed-shell (spin restricted) singlet state ([↑↓][↑↓][]). We have carried out geometry optimisation of the interstitial oxygen species in the three states described and found that:

(i) In the starting structure, the energy ordering of the three states of interstitial oxygen matches that of the oxygen atom in vacuum with the triplet lying about 0.8 eV below the closed-shell singlet and 0.3 eV below the open-shell singlet.
(ii) On relaxation of the open-shell triplet and singlet states, the oxygen atom remains on the octahedral site, while the surrounding atoms relax outward.
(iii) On a small shift off centre, the triplet and open-shell singlet octahedral configurations are restored while the closed-shell singlet undergoes a strong relaxation into a split interstitial configuration, which is 2.1 eV *lower* in energy than the initial configuration.

The two minimum-energy structures are shown in Fig. 2, with the structural parameters summarised in Table 2. Previous calculations, performed at a similar level of theory, reported the *highest energy* closed-shell singlet values for the regular octahedral neutral oxygen interstitial, resulting in much higher defect formation energies [15,16].

Analysis of the spin density of the two open-shell configurations, shown in Fig. 3 using isodensity plots, has confirmed their quasi-atomic nature and charge neutrality. The doubly occupied O 2p-like orbital, which is *not* spin polarised, is oriented along the c axis with the electron pair density attracted to the nearest Al^{3+} cations; here we observe depletion of the spin density. The spin density, of two electrons of equal spin occupying the remaining O 2p-like orbitals, is axially symmetric and forms a torus around the hexagonal c axis. The spin density of two electrons of opposite spin reveals instead the O 2p orbital like spatial distribution while retaining the axial alignment. We can also observe a weak spin polarisation of the nearest neighbour oxide ions, which is isotropic for the triplet case and anisotropic for the singlet, as spin polarisation of a pair of oxide ions by interaction with two opposite spins is cancelled by symmetry.

In the split interstitial configuration, two oxygen atoms approach each other to a close separation of 1.44 Å, which is characteristic of the peroxy species, O_2^{2-}. Therefore on relaxation, electron transfer has occurred from a lattice oxide ion to an interstitial oxygen atom, which has strongly affected their electronic structure. With respect to the two Al sites to which the interstitial is coordinated, on forming the peroxy species, the interstitial atom breaks symmetry by moving into one of the two parallel 'horizontal' oxygen planes. In the initial configuration, one Al ion is coordinated to both O_i (1.90 Å) and a lattice oxide ion (1.96 Å): on formation of the peroxy species, the Al–O_i bond length is reduced to 1.74 Å, while the Al–O_o bond length is increased to 2.63 Å. A detailed analysis of the peroxy species, which is isoelectronic with the F_2 molecule, and its role in solid oxides can be found for example in Ref. [27]. Here we note only that the ground-state is a closed-shell singlet, as we observed in the present calculations, and the usual oxide

Table 1
Physical parameters of α-alumina, including the internal degrees of freedom of the aluminium 12c (0, 0, u) and oxygen 18e (u, 0, ¼) lattice sites. Experimental data due to (a) Ref. [40] measured at room temperature and (b) Ref. [41] measured at 10 K.

	a (Å)	c (Å)	u_{Al}	u_O	E_g (eV)
Calculated	4.807	13.143	0.352	0.694	5.85
Experiment	4.759[a]	12.990[a]	0.352[a]	0.692[a]	9.25[b]

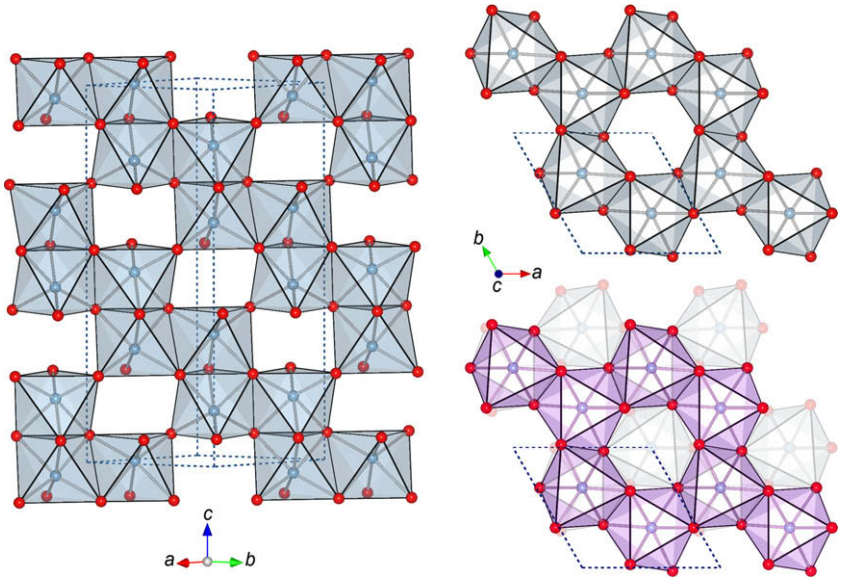

Fig. 1. Corundum crystal structure highlighting the octahedral interstitial sites. The left panel shows a rectangular octahedral layer along with the hexagonal unit cell, the top right panel shows the hexagonal octahedral layer and the bottom right panel shows two hexagonal octahedral layers superimposed. Red is reserved for O, grey for Al atoms. (For interpretation of the references to colour in this figure legend, the reader is referred to the web version of this article.)

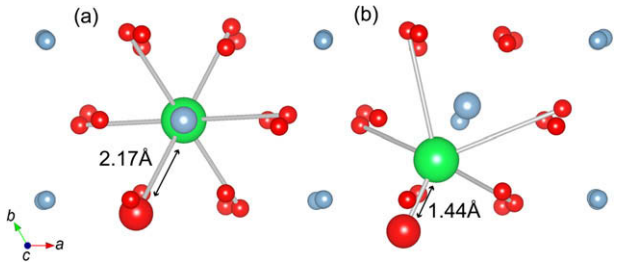

Fig. 2. Stable configurations of oxygen interstitials in corundum: (a) an octahedral site, which accommodates higher-energy triplet and open-shell singlet states, (b) a split interstitial with the ground-state closed-shell singlet. The oxygen interstitial is coloured green (large ball), and the lattice oxygen involved in the peroxide bond is enlarged. (For interpretation of the references to colour in this figure legend, the reader is referred to the web version of this article.)

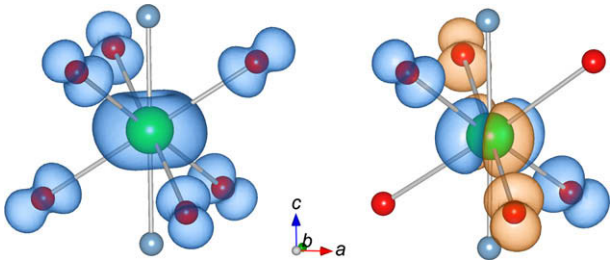

Fig. 3. Electron spin density isosurfaces of the quasi-atomic triplet configuration (left) and open-shell singlet configuration of the oxygen interstitial on the octahedral site. The positive spin density surface is shown in azure and the negative in vermillion.

Table 2
Calculated defect formation energies (Eq. (1)) and average structural parameters (in Angstrom) of oxygen interstitials in α-alumina.

	E_{form} (eV)	$d(O_i–O_O)$	$d(O_i–Al_{Al})$
Open-shell triplet	5.38	2.17	1.90
Open-shell singlet	5.68	2.17	1.89
Closed-shell singlet (TS)	6.15	2.17	1.88
Closed-shell singlet: split interstitial	4.00	1.44	1.74

and oxygen 2*p* states are transformed in the peroxy species to the occupied bonding σ and π, antibonding π* and unoccupied antibonding σ* states. In this case, new occupied states are introduced above the valence band of alumina (at 0.5 and 1.0 eV) and an unoccupied state close to the onset of the conduction band, as illustrated in the electronic density of states shown in Fig. 4. We also note the appearance of a split occupied band below the upper valence band, which is also due to the peroxy species (cf. the "3-Δ" theory of interstitial hydrogen [28]). Partitioning of the charge density associated with peroxy defect states between the interstitial and lattice oxygen atoms indicates that the highest energy defect states at the top of the valence band are dominated by the interstitial species and the lower energy states by the perturbed lattice oxygen.

It is worth noting that the formation of stable peroxide split interstitial species has been reported in other oxide systems including rock-salt MgO [29,30], wurtzite ZnO [31], rutile SnO_2 [32] and amorphous In_2ZnO_4 [33], in addition to the more open, framework structures of SiO_2 [34]. Moreover, the adsorption of atomic oxygen on the surfaces of a number of close-packed metal oxides has been studied in detail [35–38], and most recently on the (0 0 0 1) surface of corundum [39] where a stable peroxide species has been predicted. The authors have found the peroxy bond length of 1.55 Å, which is similar to our 1.44 Å, the difference being attributable to the less confining environment of the (0 0 0 1) surface, which also makes this process exothermic in contrast to the bulk environment, where it is endothermic.

The split interstitial configuration could of course also accommodate higher-energy excited states. Indeed, if we consider it as comprising two O^- ions formed after an initial electron transfer, on close approach the electrons in the singly occupied 2*p* orbitals of the O^- ion can either couple in a closed-shell singlet configuration considered above or remain uncoupled as an open-shell singlet or triplet with the lowest energy states related to the antibonding σ* state. Even higher-energy states would involve holes in the occupied antibonding π* states.

It is of particular interest to examine the transition paths connecting the lowest energy interstitial configurations. As we observed, in the ground-state the split interstitial is a singlet,

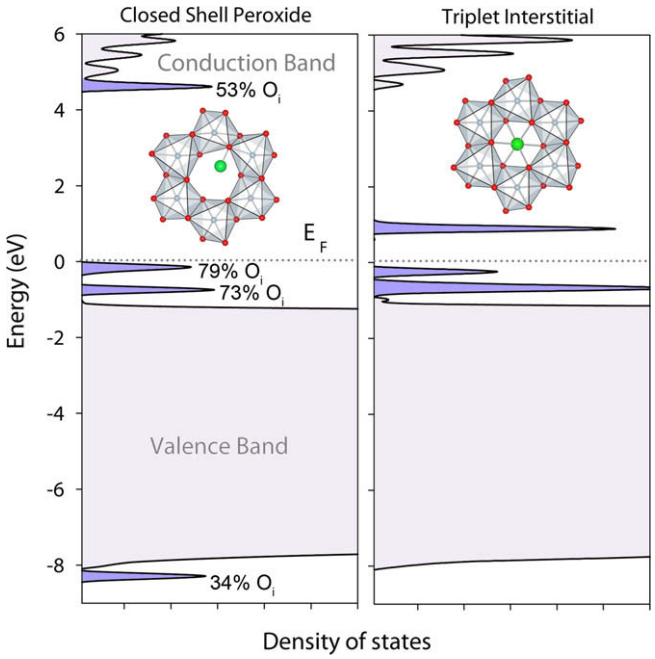

Fig. 4. Electronic density of states for the stable closed and open-shell configurations of the oxygen interstitial. The highest occupied state is set to zero as indicated by the dashed horizontal line, and split-off defect states arising from the interstitial/peroxy species are shaded blue (a fourth weak peroxy band is found to be resonant within the valence band at ca. −7.5 eV). Partitioning of the charge density associated with the peroxy defect peaks between the lattice and interstitial oxygen atoms is reported as labels next to the respective defect states.

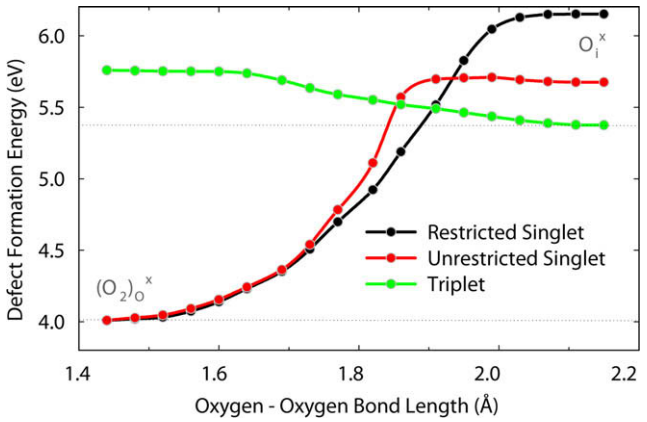

Fig. 5. Minimum-energy paths between octahedral and split interstitial sites projected on the oxygen–oxygen separation distance, obtained from NEB calculations. The three paths shown are determined by the initial state at the octahedral site: the ground-state triplet (green line), open-shell singlet (red line) and closed-shell singlet (black line). The defect formation energy is with respect to gaseous (molecular) oxygen. (For interpretation of the references to colour in this figure legend, the reader is referred to the web version of this article.)

whereas the octahedral interstitial is a triplet. We have performed NEB optimisation between the two configurations in both electronic states; the resultant energies along the minimum-energy paths are shown in Fig. 5. As we classified the states of interest using the octahedral state configurations, we will assume here that this configuration is an initial point, while the split interstitial the final. The closed-shell singlet path is a monotonic descent from a maximum to a minimum stationary point with a point of inflection at about 1.95 Å, where we expect a gradual electron transfer starts to occur. The triplet path is a monotonically increasing function, confirming the triplet as a minimum, and an extended plateau region in the peroxy stretching region, approximately [1.45, 1.65] Å. This behaviour is in contrast to more open semi-covalent silicate systems, where a triplet proves to be a metastable peroxy configuration, with a O–O separation of 1.98 Å [38]. The greater stabilisation of the peroxy for shorter distances by the more ionic Al^{3+} centre and the close proximity of a favourable alternative metastable state, in the octahedral configuration, could be identified as a source of the destabilisation of a peroxy triplet. The open-shell singlet exhibits more complex behaviour: initially its energy also monotonically, albeit very slowly, increases, but then an inflection point is found at ca. 2.0 Å. On further shortening of O-O distance to 1.95 Å a maximum is reached, after which, from about 1.85 Å, the energy rapidly drops, and at 1.7 Å the open-shell and closed-shell singlet solutions become practically indistinguishable. Thus, electron transfer to the interstitial oxygen should take place at about 1.8 Å. The overall height of the barrier is only 0.03 eV, which may be an artifact of the GGA level of theory used and more accurate electronic structure techniques will be required to ascertain the barrier height.

With regard to oxygen transport, which is of high current interest [2–4], these calculations allow us to draw only preliminary conclusions. Important alternative mechanisms should be investigated elsewhere; however, our preliminary results suggest that migration of the peroxide species is a feasible process with an activation energy of 0.73 eV across the hexagonal (1 0 0) plane. Alternatively, oxygen migration can occur via the metastable octahedral interstitial site with activation energies for the spin conserving process of about 1.7 eV and for the spin crossing process of about 1.4 eV. Both processes would involve non-radiative electronic transitions on the state crossing between a closed-shell peroxide electronic configuration and quasi-atomic open-shell configurations of the oxygen atom.

4. Conclusions

Our calculations have illustrated the complexities of oxygen interstitial structures in close-packed metal oxides by taking the example of α-alumina. Depending on the structural and spin configuration, the defect reaction energy can change by over 2 eV, which in turn will affect its equilibrium defect concentrations by many orders of magnitude. These results have direct implications for modelling defect processes in other metal oxide systems, and indicate that the diffusion processes in such materials may be more complicated than has been previously assumed, where the role of peroxy species could be critical.

Acknowledgements

This work made use of the facilities of HECToR, the UK's national high-performance computing service via our membership of the UK's HPC Materials Chemistry Consortium, which is funded by EPSRC (EP/F067496). A.W. would like to acknowledge funding from a Marie-Curie Intra-European Fellowship from the European Union under the Seventh Framework Programme. The work has also been supported by an EPSRC Portfolio Partnership (Grant No. ED/D504872).

References

[1] D.M. Smyth, The Defect Chemistry of Metal Oxides, Oxford University Press, Oxford, 2000.
[2] A.H. Heuer, J. Eur. Ceram. Soc. 28 (2008) 1495.
[3] K. Moritani, Y. Teraoka, I. Takagi, M. Akiyoshi, H. Moriyama, J. Nucl. Mater. 373 (2008) 157.
[4] A. Morono, E.R. Hodgson, J. Nucl. Mater. 307 (2002) 1246.
[5] J.H. Crawford Jr., J. Nucl. Mater. 108–109 (1982) 644.

[6] C.R.A. Catlow, R. James, W.C. Mackrodt, R.F. Stewart, Phys. Rev. B 25 (1982) 1006.
[7] G.J. Dienes, D.O. Welch, C.R. Fischer, R.D. Hatcher, O. Lazareth, M. Samberg, Phys. Rev. B 11 (1975) 3060.
[8] R.W. Grimes, J. Am. Ceram. Soc. 77 (1994) 378.
[9] U. Aschauer, P. Bowen, S.C. Parker, Acta Mater. 57 (2009) 4765.
[10] P.W.M. Jacobs, E.A. Kotomin, Philos. Mag. A – Phys. Condens. Matter Struct. Defect Mech. Prop. 68 (1993) 695.
[11] P.W.M. Jacobs, E.A. Kotomin, J. Solid State Chem. 106 (1993) 27.
[12] E.A. Kotomin, A. Stashans, P.W.M. Jacobs, Radiat. Eff. Defects Solids 134 (1995) 87.
[13] J.T. Devreese, V.M. Fomin, E.P. Pokatilov, E.A. Kotomin, R. Eglitis, Y.F. Zhukovskii, Phys. Rev. B 63 (2001) 6.
[14] P.W.M. Jacobs, E.A. Kotomin, J. Am. Ceram. Soc. 77 (1994) 2505.
[15] K. Matsunaga, T. Tanaka, T. Yamamoto, Y. Ikuhara, Phys. Rev. B 68 (2003) 085110.
[16] N.D.M. Hine, K. Frensch, W.M.C. Foulkes, M.W. Finnis, Phys. Rev. B 79 (2009) 024112.
[17] J.R. Weber, A. Janotti, C.G. Van de Walle, Microelectron. Eng. 86 (2009) 1756.
[18] D. Liu, S.J. Clark, J. Robertson, Appl. Phys. Lett. 96 (2010) 032905.
[19] C. Freysoldt, J. Neugebauer, C.G. Van de Walle, Phys. Rev. Lett. 102 (2009) 016402.
[20] A.A. Sokol, S.T. Bromley, S.A. French, C.R.A. Catlow, P. Sherwood, Int. J. Quantum Chem. 99 (2004) 695.
[21] P. Sherwood et al., J. Mol. Struct.: THEOCHEM 632 (2003) 1.
[22] G. Kresse, D. Joubert, Phys. Rev. B 59 (1999) 1758.
[23] G. Kresse, J. Furthmüller, Phys. Rev. B 54 (1996) 11169.
[24] J.P. Perdew, K. Burke, M. Ernzerhof, Phys. Rev. Lett. 77 (1996) 3865.
[25] P.E. Blöchl, Phys. Rev. B 50 (1994) 17953.
[26] G. Mills, H. Jónsson, G.K. Schenter, Surf. Sci. 324 (1995) 305.
[27] M. Königstein, A.A. Sokol, C.R.A. Catlow, Phys. Rev. B 60 (1999) 4594.
[28] S.F.J. Cox, J.L. Gavartin, J.M. Gil, R.C. Vilao, J.S. Lord, E.A. Davis, Physica B 376 (2006) 385.
[29] R.A. Evarestov, P.W.M. Jacobs, A.V. Leko, Phys. Rev. B 54 (1996) 8969.
[30] E.A. Kotomin, A.I. Popov, Nucl. Instrum. Methods Phys. Res., Sect. B 141 (1998) 1.
[31] C.R.A. Catlow, S.A. French, A.A. Sokol, A.A. Al-Sunaidi, S.M. Woodley, J. Comput. Chem. 29 (2008) 2234.
[32] K.G. Godinho, A. Walsh, G.W. Watson, J. Phys. Chem. C 113 (2009) 439.
[33] A. Walsh, J.L.F. Da Silva, S.-H. Wei, Chem. Mater. 21 (2009) 5119.
[34] A.M. Stoneham, M.A. Szymanski, A.L. Shluger, Phys. Rev. B 63 (2001) 241304.
[35] L.N. Kantorovich, M.J. Gillan, J.A. White, J. Chem. Soc. – Faraday Trans. 92 (1996) 2075.
[36] C. Di Valentin, R. Ferullo, R. Binda, G. Pacchioni, Surf. Sci. 600 (2006) 1147.
[37] P.V. Sushko, A.L. Shluger, C.R.A. Catlow, Surf. Sci. 450 (2000) 153.
[38] S.T. Bromley, S.A. French, A.A. Sokol, P.V. Sushko, C.R.A. Catlow, Recent Advances in Density Functional Methods (Part III), World Scientific, London, 2002.
[39] P. Gamallo, R. Sayos, Phys. Chem. Chem. Phys. 9 (2007) 5112.
[40] P. Thompson, D.E. Cox, J.B. Hastings, J. Appl. Crystallogr. 20 (1987) 79.
[41] T. Tomiki et al., J. Phys. Soc. Jpn. 62 (1993) 573.